Journal of the Korean Society for Nondestructive Testing
Vol. 30, No. 3 (2010. 6)

An Application of a Magnetic Camera for an NDT System for Aging Aircraft

Jungmin Kim*, Jongwoo Jun**, Jaesun Lee* and Jinyi Lee***†

Abstract The usefulness of the magnetic camera for non-destructive testing of aging aircraft is discussed in this paper. The magnetic camera can be used f magnetic particle testing(MT), magnetic flux leakage testing(MFLT), eddy current testing(ECT) and penetration testing(PT). It measures the distribution of a magnetic field and visualizes the magnetic pattern. Near and far side cracks, fatigue, thickness degradation, and cracks under rivets have been detected. The possibility of quantitative evaluation was also examined. Using indirect experiments, we verified the detection ability of the sensor for cracks in titanium and advanced composite materials.

Keywords: Magnetic Camera, Non-Destructive Testing, Crack, Aircraft

1. Introduction

On August 12th, 1985, 520 lives, including 15 cabin crewmembers, on board Japan Airlines No.123(Boeing 747SR-46) were lost because of an accident(Gero, 1994). This accident was due to multisite cracks, which occurred at the riveting points between the upper and lower fuselage. This was a tragedy, not only for the economical loss, but also in the lives lost due to small damages.

The main cause for the damage was the deterioration of materials, initiating and propagating cracks in aging aircraft, nuclear and thermal power generation plants, rockets, and integrated circuit(IC) packages. The initiation of these defects was due to (1) inclusions in the raw material, and (2) a hostile environment for operation which promotes corrosion, fatigue and thermal degradation. The defects were inspected by using pre-service inspection(PSI) and in-service inspection(ISI), respectively. The aircraft mentioned above was damaged due to another accident, which occurred 7 years before the fatal accident. There was a weaker riveting than the maintenance code required after the first accident. The cracks were initiated and propagated during the 12,319 times of taking off and landing during those 7 years(Gero, 1994). However, the cracks were not detected in-spite of six ISIs.

Military aircraft operate under harsher environments than civilian aircraft, seeing larger differences of temperature during maneuvers, operation in bad weather, fatigue due to changes in loading, and corrosion. Correspondingly, the rapid and accurate inspection of cracks in aging military aircraft is necessary for safeguarding the life of the pilot, saving the armaments, and maximizing the utility of military strength. The

Received: March 18, 2010, Revised: June 4, 2010, Accepted: June 10, 2010. *Department of Control and Instrument Engineering Graduate School of Chosun University, **Research Center for Real Time NDT Chosun University, ***Department of Control, Instrument and Robot Engineering, Chosun University, 375, Seosuk-dong, Dong-gu Gwangju 501-759, Republic of Korea, †Corresponding Author: jinyilee@chosun.ac.kr

field application of an ISI system according to the kinds of material, shape and construction, the easy conservativeness for the maintenance of the ISI system, and an easy adaptation needed for diverting of one system into another ISI system are necessary properties for an independent national defense capability. However, over 95 % of the non-destructive testing(NDT) equipment is imported to Korea. The standard of the technology and the equipment compared to an advanced country are under 50 % and 30 %, respectively(Korea Association for Nondestructive testing, 2004). Correspondingly, a state-of-the-art non-destructive testing method using our own technology and our own patents has to be secured and nurtured to satisfy the above-mentioned field application, conservation, and reconstruction.

The magnetic camera is its own technology, which can be used instead of magnetic particle testing(MT), magnetic flux leakage testing(MFLT), eddy current testing (ECT), and penetration testing(PT). It measures the distribution of a magnetic field and visualizes the magnetic pattern. We reviewed the magnetic camera as an ISI system for inspecting and evaluating cracks on aging aircraft. Several kinds of cracks on an aluminum alloy plate, the riveting construction, and inconel plates were used to verify the effectiveness of the magnetic camera as a state-of-the-art NDT technology.

2. The Magnetic Camera System

The magnetic camera consists of a magnetic source, a magnetic sensor array, a magnetic lens, circuitry including analog-to-digital(AD) converters, an interface, a computer, and a display, as shown in Fig. 1. Sometimes we use a microprocessor instead of a computer. The magnetic source, consisting of a direct magnetic field (Hwang et al., 2009; Lee et al., 2008a), an alternating magnetic field, an electrical field, an induced current, an area-type induced current (Jun and Lee, 2008) or terrestrial magnetism (Lee et al., 2004c) are applied to the objects. The magnetic field is distorted according to the existence of metal or cracks. Because of this distortion, the distribution of the magnetic field in the air is changed, and concentrated onto the magnetic lens(Lee and Hwang, 2006a). The distribution of the magnetic field can be translated into analog signals by using the magnetic sensor array. The digital signals, which are translated from the analog signals by using the AD converters, are inputted to the computer, stored, processed and displayed. The kinds and principles of the magnetic sources, sensor array, electrical circuits and AD converters will be explained in the following subsections.

The authors have developed optimized magnetic sources for inspecting cracks on several materials and objects. These sources are the cross-type magnetic flux leakage(C-MFL)(Lee and Hwang, 2006b), the direct current magnetic flux leakage (DC-MFL)(Lee et al., 2008a), the plate-type magnetic flux leakage(P-MFL)(Lee et al., 2008d), the in-side solenoid magnetic flux leakage (IS-MFL)(Lee et al., 2008d), the vertical-type magnetic flux leakage(V-MFL)(Lee et al., 2004b), the sheet-type induced current(STIC)(Jun and Lee, 2008b), the improved sheet-type induced current(i-STIC)(Lee and Jun, 2008b), the combined induced current and magnetic flux leakage(CIC-MFL)(Jun et al., 2007a), and the magnetic fluid penetration testing(MFPT)(Lee and Jun, 2008a) methods. The properties of each magnetic source are given in Table 1.

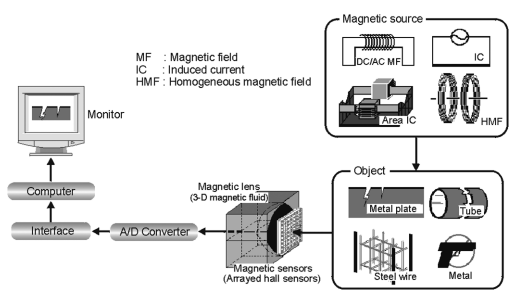

Fig. 1 Consistence of magnetic camera

Table 1 The magnetic sources and their properties

Full name	Abbreviation	Objective	Properties	Applications
Cross-type magnetizer	C-MFL	Ferromagnetic material	Inspection cracks with any length direction	ISI of steel construction
Direct current yoke-type magnetizer	DC-MFL	Ferromagnetic material	Compact sized ISI system. Optimized for the scan-type magnetic camera	PSI of steel manufacturing process and ISI of express train wheel
Plate-type magnetizer	P-MFL	Ferromagnetic material	Suitable for inspecting cracks in the pipeline. Optimized for the cylinder-type magnetic camera	ISI in the pipelines and PSI of the wire manufacturing
Inside solenoid-type magnetizer	IS-MFL	Ferromagnetic material		ISI in the steel pipelines
Vertical-type magnetizer	V-MFL	Ferromagnetic material, paramagnetic metal, and combined material	Suitable for detecting metal. Optimized for the hand-held metal detector	ISI in the aircraft, the nuclear- and thermal power generation plants
Sheet-type induced current	STIC		Inspecting cracks on the any metal. Optimized for the area-type magnetic camera	
Improved sheet-type induced current	i-STIC		Inspecting cracks on the metal. Optimized for the scan-type magnetic camera	
Complex induced current and magnetic flux leakage	CIC-MFL			PSI in the (stainless) steel manufacturing process and ISI in the aircraft and power generation plants
Magnetic fluid penetration testing	MFPT	Any material	Open cracks on the surface	ISI in the aircraft and power generation plant

The crack detection ability of the MFLT and MT methods can be reduced when the crack direction is parallel to the magnetization direction. In order to improve the crack detection ability for the MFLT or MT methods, we propose the cross-type magnetic source(Lee and Hwang, 2006b). It consists of 2 pairs of poles. Each pole faces each other in pole pairs. The pairs of poles are positioned in the vertical direction in the cross-type magnetizer. Each pair of poles is operated with alternating current. Correspond- ingly, cracks going in any direction can be detected.

A small yoke-type magnetizer is positioned at the back-side of the sensor array in the DC-MFL method. We inspected and evaluated the position, shape, direction, length and volume of cracks on the billet and the express wheel using the DC-MFL(Lee et al., 2008a; Smith et al., 2003). The P-MFL and IS-MFL sources can be used for inspecting cracks in pipelines.

A sheet-type current can be induced in the specimen by using the STIC and i-STIC. An alternating magnetic field occurs in the core (②) when alternating current is input to the primary coil (①) of the STIC, as shown in Fig. 2(a). Correspondingly, an alternating sheet-type current is induced in the copper sheet (③), which passes through the core (②). The sheet-type current then induces current in a specimen (④) under the copper sheet. Because of the current distortion due to a crack, the distribution of the magnetic field is changed. The i-STIC, as shown in Fig. 2(b), can generate a larger induced current than the STIC. It is useful for the scan-type magnetic camera. The STIC is suitable for use by the area-type magnetic camera. The distorted magnetic field can be measured by using the Hall sensor array, and so reveal cracks on ferromagnetic, paramagnetic and combined

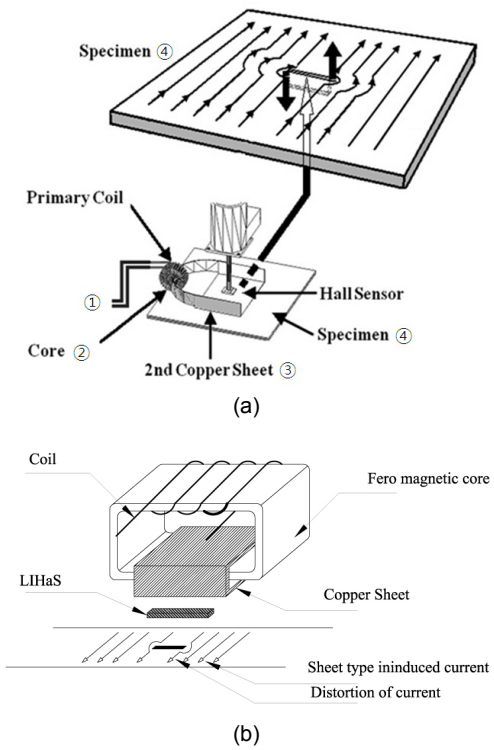

Fig. 2 Principle of induced current; (a) Sheet-type induced current (STIC), (b) Improved sheet-type induced current (i-STIC)

materials. The crack detection ability is excellent in metals with a high conductivity. Fatigue cracks in aluminum alloys and the magnesium plates have been detected.

The combined induced current and magnetic flux leakage(CIC-MFL) is similar to the DC-MFL, as shown in Fig. 3(a). The magnetic field occurs when alternating current is input to the coils, which are wound around the poles of the magnetizer, as shown in Fig. 3(b). The current is induced in the vertical direction with the magnetic field, as shown in Fig. 3(c). If the crack direction is vertical with the magnetization direction, the leakage magnetic flux is maximized in the ferromagnetic material. If the crack length direction is parallel to the magnetization direction, the distortion of the induced current is also maximized. Correspondingly, we can detect cracks in any direction by using the CIC-MFL on ferromagnetic materials. The CIC-MFL is also useful for inspecting cracks on paramagnetic materials using induced current. The crack inspection ability is maximized when the length of the crack is vertical to the direction of the induced current.

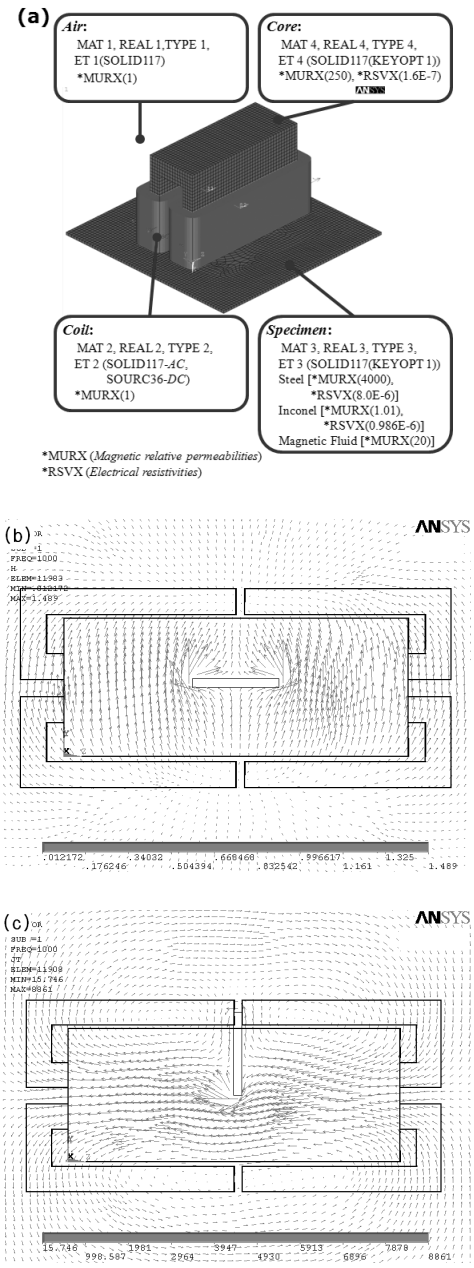

Fig. 3 Principles of CIC-MFL; (a) Construction, (b) Magnetic field generation, (c) Electrical field generation

Hall sensors, magnetic resistance(MR) sensors, and giant magnetic resistance(GMR) sensors can be used as the magnetic sensor used to measure the distribution of a magnetic field. The GMR sensor is based on the GMR effect, which won a Nobel Prize in 2007. Several papers have reported that the GMR sensor can be used in the NDT field because of its small size and high sensitivity(Dogaru and Smith, 2001; Smith et al., 2003). We have been using Hall Effect sensors for the magnetic sensor in the NDT field because of their full scale operational region(FSO) and sensitivity. The FSO is about ±4 mT when the output is amplified to 59.2 dB, which is a larger FSO than the GMR sensor or the spin dependent tunneling(SDT) sensor by about 5~10 times. The sensitivity is 2.51 V/mT, which is a larger sensitivity than the GMR sensor or the SDT sensor by about 10~100 times. The standard deviation is about 0.01 V and the measurement precision is under 4 μT. Therefore, we use Hall sensors as the magnetic sensor in the magnetic camera system. According to the sensor array and scanning method, the magnetic camera is classified into three categories.

(1) Single sensor scanning(SSS). The distribution of magnetic field can be measured by using a sensor by scanning on the 2-dimensional surface with a precision scanning machine.
(2) Linearly integrated Hall sensors array(LIHaS). The linearly integrated Hall sensor array is used for measuring the distribution of a magnetic field. Hall sensors are arrayed on the same wafer in a matrix.
(3) Area-type integrated Hall sensors array (AIHaS). The sensors are arrayed on a wafer or a PCB in a matrix. Basically, we don't need to scan the sensors.

The spatial resolutions of the SSS, the LIHaS and the AIHaS are 0.5 mm, 0.52 mm and 0.78 mm, respectively, developed in our laboratory. The plate and cylinder types of the AIHaS have also been developed. Fig. 4 shows examples of the visualized distribution of a magnetic field around a clip (Fig. 4(a)) and in a pipeline (Fig. 4(b)). 1,024 Hall sensors are arrayed on the same wafer and on the surface of the cylindrical printed circuit board (PCB). The spatial resolutions of these AIHaSs are 0.52 mm and 3.5 mm, respectively.

There are 2 pins used for the input and 2 pins used for the output in a Hall sensor. A stable voltage or current is applied to the input lines. The outputs, that is, the Hall voltages from each pin, increase or decrease proportionally to the intensity of the magnetic field. A differential op-amp is used to measure the intensity of the magnetic field detected by the Hall sensor. A high pass filter(HPF) and a low pass filter(LPF) are used to extract the signal with a certain frequency, and for removing the noise. The frequency of the Hall voltage coincides with the input alternating current of the CIC-MFL, STIC and i-STIC. The phase delay and the signal

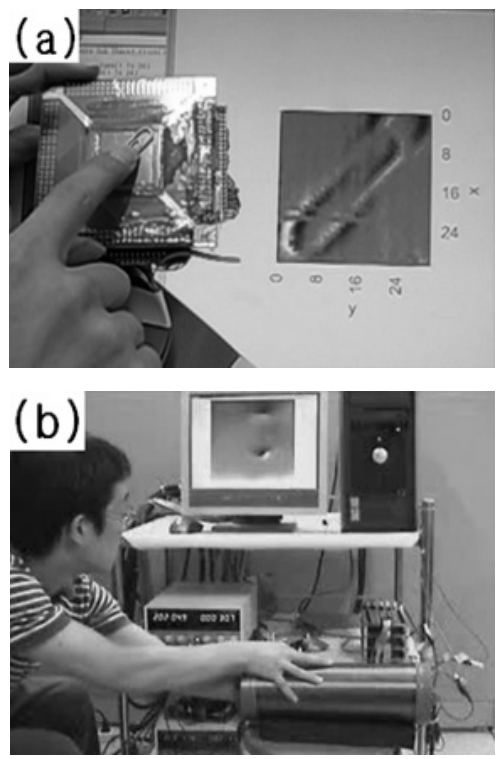

Fig. 4 Visualization of the distribution of magnetic field using AIHaS with; (a) High spatial resolution on a wafer and (b) Low spatial resolution on the cylindrical-shape PCB

amplitude are important in estimating the crack's existence and size. We developed a root-mean-square(RMS) circuit and used it for extracting the amplitude of the Hall voltage(Jun and Lee, 2008; Jun et al., 2007a; Jun et al., 2007b).

3. The Experiment and Discussion

3.1 The Specimens

The specimens, composed of aluminum alloy, are used for verifying the magnetic camera as an NDT system, as shown in Figs. 5 through 9 and Table 2.

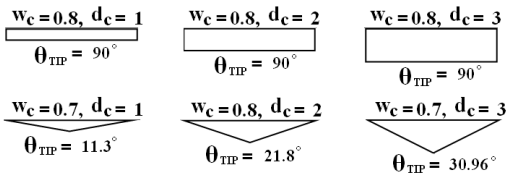

Fig. 5 Several shapes and sizes of the plate-type specimens (PLT-Near and PLT-Far)

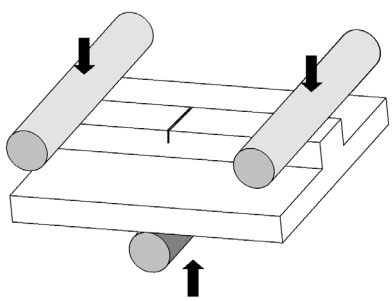

Fig. 6 Fatigue cracks (FTG)

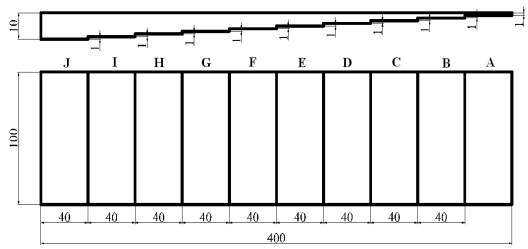

Fig. 7 Wall loss (WT)

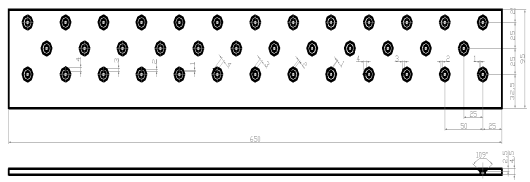

Fig. 8 Rivet specimen (RVT-PLT)

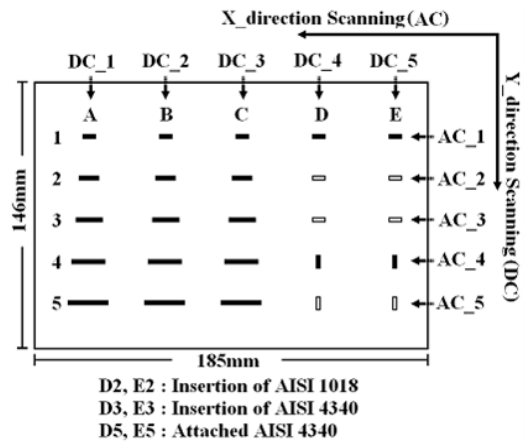

Fig. 9 Inconel specimen (ICN)

Table 2 The shapes and objectives for each crack

specimen	abbreviation	magnetic source	sensor type	size of specimen [mm]	size of cracks [mm]	Applications (objectives)
Plate	PLT	CIC-MFL	LIHaS	200x200x5	(1~3) of depth	Near- and far-side on the fuselage
Fatigue	FTG	CIC-MFL	LIHaS	100x200x5	(9.75, 22) of length	Fatigue on the wing
Wall loss	WT	V-MFL, CIC-MFL	SSS/ LIHaS	100x400x10	(1~10) of thickness	Corrosion in the fuselage and the wing
Rivet plate	RVT-PLT	CIC-MFL	LIHaS	95x650x4.5	(1.5, 3, 4.5, 5) of length	Multisite cracks under the rivet
Inconel 600	ICN	MFPT (DC-MFL, CIC-MFL)	LIHaS	146x185x2	0.12 width and (2~10) of length and (0.2~0.6) of depth	Cracks on the fire resistance wall and the landing wheel

4. The Results and Discussions

4.1 The Near-Side and Far-Side Cracks

Artificial cracks with the length of 10 mm, width of 0.7 mm and depth of 1, 2, 3 mm with rectangular and triangular shapes were formed using electro-discharge machining(EDM) on the center of the specimen with the size of 200*200*5 mm^3 (PLT), as shown in Fig. 5. The magnetic images at the lift-off 1 mm on the near-side and far-side were obtained using by the CIC-MFL and a LIHaS consisting of 64 Hall sensors.

The surface cracks could be detected when the direction of the crack was not only parallel with scanning (Fig. 10), but also vertical (Fig. 11), as shown in Fig. 10 and Fig. 11. The distribution of the magnetic field on a crack is similar with shape of crack, as shown in Fig. 10. That is, the sectional views of the magnetic field are similar with the rectangular and triangular shapes. The intensity of each distribution changes in proportion to the depth of the crack. The length of the rectangular crack can be estimated from the magnetic images. That is, the distance between the two largest distortions on the tips of the crack indicates the length of the rectangular crack. Let us call this distance the tip-distance.

On the other hand, the tip-distance is smaller than the real crack length in the triangular crack. However, we can know the shape of the crack by using the images found in Fig. 10(b). The length of the crack can be estimated if we know the shape of the crack. In addition, the maximum value of the distribution of the magnetic field, when the scanning direction is parallel with the crack length direction as shown in Fig. 10, is about 50 % in the case of the vertical direction, as shown in Fig. 11. Figs. 12 and 13 show the inspection results, which examined the far-side crack of the same specimen (PLT). If the length of the crack is

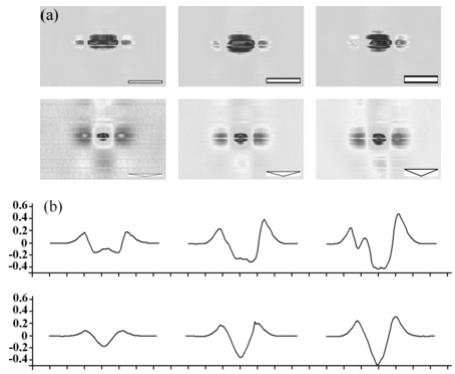

Fig. 10 The near-side crack inspection results when the length direction of crack is parallel with the scanning direction; (a) Magnetic images, (b) Distribution of magnetic field on the center of crack

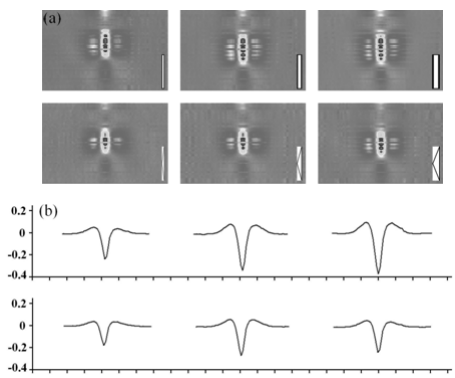

Fig. 11 The near-side crack inspection results when the length direction of crack is vertical to the scanning direction; (a) Magnetic images, (b) Distribution of magnetic field on the center of crack

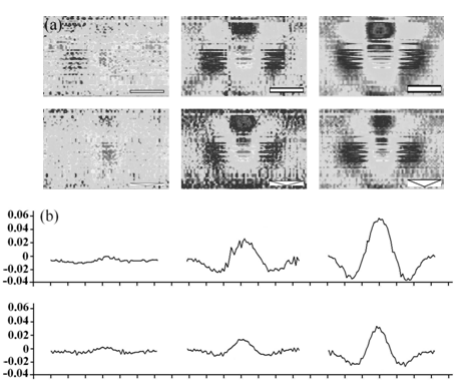

Fig. 12 The far-side crack inspection results when the length direction of crack is parallel with the scanning direction; (a) Magnetic images, (b) Distribution of magnetic field on the center of crack

parallel to the scanning direction, not only the rectangular cracks, but also the triangular cracks with the depth of 2 mm can be detected, as shown in Fig. 12(a). That is, the crack caused by corrosion, which is positioned at the depth of 3 mm from the surface, can be detected by using the proposed method. When the crack length direction is vertical to the scanning, as shown in Fig. 13(a), the intensity of magnetic field is weak. The cracks can be detected when the depth is over 3 mm. That is, the crack, which is positioned at the depth of 2 mm from the surface, can be detectable. The crack with a depth of 2 mm can be detected using the section view shown in Fig. 13(b).

The volume of the crack can be estimated by using the following equation(Hwang et al., 2009; Jun and Lee, 2008; Lee et al., 2008a; Lee et al., 2008e):

$$\frac{\partial V_H}{\partial C_{Total}} = \sum_{i=1}^{L_C/2S}\left[\mathrm{Max}\left(\frac{\partial V_{Hi}}{\partial C}\right) + \left|\mathrm{Min}\left(\frac{\partial V_{Hi}}{\partial C}\right)\right|\right] \quad (1)$$

The LC and S express the length of the crack, which can be estimated by using the tip-distance, and the resolution of the magnetic camera system, respectively. C is the scanning direction. Fig. 14 shows the relationship between the $\partial VH/\partial C|_{Total}$, which is calculated by eqn. (1) and the section area. This result indicates that the crack can be evaluated quantitatively.

4.2 The Fatigue Crack Inspection

The fatigue crack was propagated from an initial slit on a convex specimen propagated by using a three point bending fatigue method, as shown in Fig. 6. After the generation of the fatigue crack in the specimen, the convex-part was cut. The two resulting specimens, which have the lengths of 9.75 mm and 22 mm, respectively, on the center of specimen (100*200*5 mm^3) size were examined. The lift-off is 1 mm. The CIC-MFL and the LIHaS with 64 Hall sensors were used to inspect the cracks. As shown in Fig. 15, the fatigue cracks could be detected at both the near-side and the far-side. In addition, the crack length can be estimated by using the tip-distance.

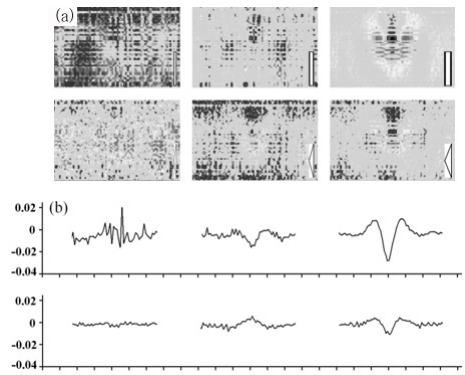

Fig. 13 The far-side crack inspection results when the length direction of crack is vertical to the scanning direction; (a) Magnetic images, (b) Distribution of magnetic field on the center of crack

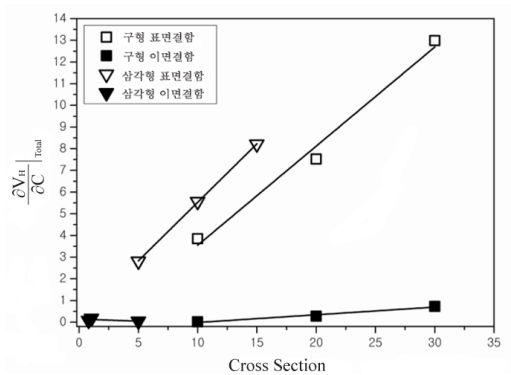

Fig. 14 Estimation of crack section area using the proposed evaluation algorithm

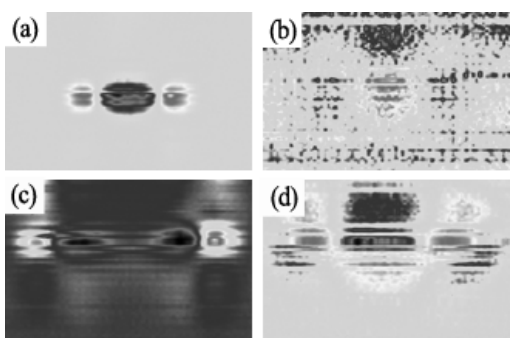

Fig. 15 Fatigue crack inspection; (a) Surface crack with 9.75 mm length, (b) Far-side crack with 9.75 mm, (c) Surface crack with 22 mm length, (d) Far-side crack with 22 mm length

4.3 The Wall Loss Inspection

Fig. 16 shows the distribution of the magnetic field, which is obtained using V-MFL and SSS, on the far-side of the wall loss specimen (100*400*10 mm^3). A wall loss of 90 %, 80 % and 70 % was distinguished. That is, the loss, which is positioned at the 3 mm depth, can be detected. It is because the skin depth is about 2.9 mm in the aluminum alloy. Also, Fig. 17 shows the distribution of the magnetic field, which is obtained by using the CIC-MFL and the LIHaS. The loss position could be detected.

4.4 The Riveting Crack Inspection

Fig. 8 shows the rivet specimen (RVT-PLT). The thickness of upper specimen is 3 mm, and the head angle of the rivet is 109°. Cracks with 1.5, 3, 4.5 and 5 mm of length were introduced under the rivet head. The length direction of each crack is parallel and 45° with the scanning direction. The rivets are set in the rivet hole for examination. The current is induced in the vertical direction along with the scanning direction. The induced current distorted around the rivet; the intensity of magnetic field is maximized at the tips of the rivet, as shown in Fig. 18(a). The differential process results $\partial V/\partial x$

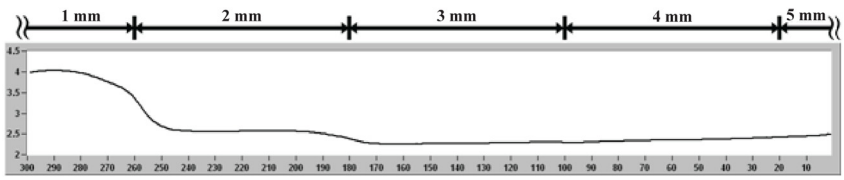

Fig. 16 Distribution of magnetic field, which is obtained using V-MFL and SSS

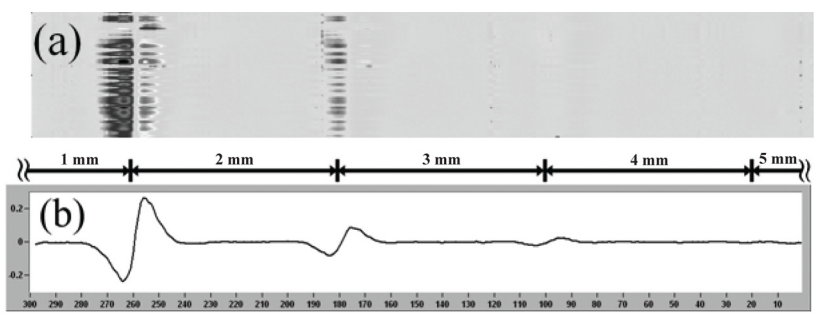

Fig. 17 Distribution of magnetic field, which is obtained using CIC-MFL and LIHaS

Fig. 18 In the case of no crack; (a) Normal, (b) $\partial V/\partial x$, (c) Image processing

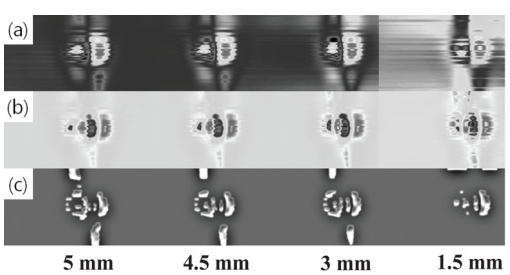

Fig. 19 In the case of crack with parallel to the scanning direction; (a) Normal, (b) $\partial V/\partial x$, (c) Image processing

images are shown in Fig. 18(b). Fig. 18(c) shows the image processing results, that is, multiplying (a) with (b), the plaster and the high pass filtering. We obtained a similar three patterns on the rivet without a crack.

The processed magnetic images on the rivet with cracks, as shown in Fig. 19(c), provide different patterns when compared to Fig. 18(c). The crack with the length of 1.5 mm cannot be detected. However, if the crack length is over 3 mm, that is, out of the rivet head, the pattern is different to Fig. 18(c). Also, if the crack direction is 45° with the scanning direction, the pattern shows the direction of the crack, as shown in Fig. 20(c).

4.5 The Crack Inspection on the Titanium Alloy

Titanium alloy has a strength similar to steel alloy. It is much lighter than iron, and the corrosion resistance is better than stainless steel. The strength can be maintained at 200~500 ℃. Correspondingly, titanium alloy is a very important material used in the aircraft. Aluminum alloy cannot be used as the fuselage of an aircraft at a 10 km altitude flying at Mach 2.7, therefore titanium alloy has to be used in this case(Japan Aeronautic Association, 1993). It is also used in engine parts and in the main leg part of a Boeing 747, and for many parts in our fighting aircraft.

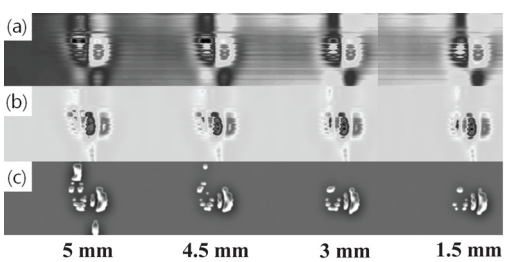

Fig. 20 In the case of crack with 45° to the scanning direction; (a) Normal, (b) $\partial V/\partial x$, (c) Image processing

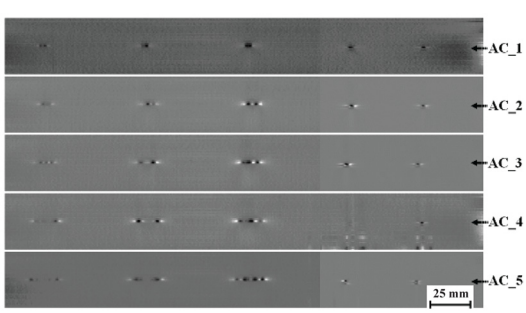

Fig. 21 Inspection results of crack on the inconel specimen

The relative permeability and electrical conductivity of titanium are 1 and $1.82*10^6$ s/m, respectively. The electrical conductivity is about 1/20~1/30 compared to aluminum ($3.82*10^7$ s/m) and copper ($5.08*10^7$ s/m). Also, it is half that of iron ($3.8*10^6$ s/m). It means that titanium has difficulty in conducting current. In addition, if an alternating current, used for inducing eddy currents, is applied in titanium, there is heat. On the other hand, the electrical conductivity of inconel is $0.986*10^6$ s/m, similar to titanium. Therefore we used an inconel specimen instead of titanium because of its low price. Artificial cracks with 0.12 mm of width, 0.2, 0.4, 0.6 mm of depth, 2, 4, 6, 8, 10 mm of length were introduced using the EDM on a inconel specimen ($146*185*2$ mm^3), as shown in Fig. 9. The magnetic fluid penetrated each crack(Lee and Jun, 2009). The magnetic images were obtained using the CIC-MFL and the LIHaS, as shown in Fig. 21. As shown in the results, the cracks having a greater width than 0.12 mm, depth of 0.2 mm and length of 2 mm were detected.

5. Conclusion

Over 95 % of non-destructive testing(NDT) equipment is imported to Korea. The standards of technology and equipment compared with an advanced country are under 50 % and 30 %, respectively. Correspondingly, state-of-the-art non-destructive testing methods using our own technologies with our own patents have to be secured and nurtured for satisfying field applications, conservativeness and reconstruction. The magnetic camera is our own technology,

which can supplement the weakness of MT, MFLT, ECT and PT. We consider the application possibility of the magnetic camera as an NDT system for aging aircraft, and obtained conclusions as follows:

(1) A surface crack on the aluminum alloy specimen (Al7075) with 1 mm of depth can be detected. Also, the far-side crack, which is positioned at the depth of 3 mm, can be detected. In addition, the crack volume can be estimated. This result can be used for inspecting and for the evaluation of corrosion.
(2) A fatigue crack on the aluminum alloy specimen (Al7075) with the length of 9.75 mm can be detected at the near and far side.
(3) A wall loss within 3 mm can be detected and evaluated. Additionally, the boundary of the wall loss can be visualized.
(4) A hidden crack under a rivet with the length of 3 mm can be detected. It isn't necessary to remove the paint to inspect a crack.
(5) Cracks on the inconel specimen can be detected by the penetrating magnetic fluid method. This idea can be used for the inspection of cracks in titanium alloy.

Acknowledgements

This research was supported by the MKE (The Ministry of Knowledge Economy), Korea, under the ITRC(Information Technology Research Center) support program supervised by the NIPA(National IT Industry Promotion Agency) (NIPA-2010-C1090-1021-0013). We are grateful of support.

References

Gero, D (1994) *Aviation Disasters*, Icarus press, Japan, pp. 187-190

Korea Association for Non-destructive Testing (2004) *A Study on Safety Management and Promotion System for NDT*, Ministry of Education, Science and Technology, Korea

Japan Aeronautic Association (1993) *Aircraft Materials*, Japan

Choi, S. H., Hwang, J. S., Jun, J. W., Lee, J. Y. and Kim, C. W. (2007) Improvement of Crack Detection Probability by Using Magnetic Camera and Image Processing, *Key Engineering Materials*, 353-358, pp. 2375-2378

Dogaru, T. and Smith, S. T. (2001) Giant Magnetoresistance-Based Eddy-Current Sensor, *IEEE Trans Magn*. Vol. 37, No. 5, pp. 3831-3838

Hwang, J. S., Lee, J. Y. and Kwon, S. J. (2009) The Application of a Differential Type Hall Sensors Array to the Nondestructive Testing of Express Train Wheels, *NDT & E International*, Vol. 42, No. 1, pp. 34-41

Hwang, J. S., Jun, J. W., Choi, S. H., Kim, C. W., Ogawa, K. and Lee, J. Y. (2007) A Study of Magnetic Charge per Unit Area of Dipole Model for the NDE, *Key Engineering Materials*, 353-358, pp. 2371-2374

Hwang, J. S. and Lee, J. Y. (2006) Modeling of a Scan Type Magnetic Camera Image Using the Improved Dipole Model, *Journal of Mechanical Science and Technology*, Vol. 20, No. 10, pp. 1691-1701

Jun, J. W. and Lee, J. Y. (2008) Nondestructive Evaluation of a Crack on Austenitic Stainless Steel Using the Sheet Type Induced Current and the Hall Sensor Array, *Journal of Mechanical Science and Technology*, Vol. 22, No. 9, pp. 1684-1691

Jun, J. W., Lee, J. Y. and Park, D. K. (2007a) NDT of a Nickel Coated Inconel Specimen

Using by the Complex Induced Current – Magnetic Flux Leakage Method and Linearly Integrated Hall Sensor Array, *Journal of the Korean Society for Nondestructive Testing*, Vol. 27, No. 5, pp. 375-382

Jun, J. W., Hwang, J. S., Kim, K. J., Ogawa, K. and Lee, J. Y. (2007b) Development of Signal Processing Circuit of a Magnetic Camera for the NDT of a Paramagnetic Material, *Key Engineering Materials*, 353-358, pp. 2379-2382

Lee, J. Y. and Hwang, J. S. (2006a) The Detection Probability Improvement of the Far-Side Crack on the High Lift-off Using the Magnetic Camera, International *Journal of Modern Physics B*, Vol. 20, Nos. 25-27, pp. 4631-4636

Lee, J. Y. and Hwang, J. S. (2006b) A Study of the Quantitative Nondestructive Evaluation Using the Cross Type Magnetic Source, *Key Engineering Materials*, 321, pp. 1447-1450

Lee, J. Y., Hwang, J. S., Jun, J. W. and Choi, S. H. (2008a) Nondestructive Testing and Crack Evaluation of Ferromangetic Material by Using the Linearly Integrated Hall Sensor Array, *Journal of Mechanical Science and Technology*, Vol. 22, pp. 2310-2317

Lee, J. Y., Jun, J. W. and Hwang, J. S. (2008b) Magnetic Sensor Array and Apparatus for Detecting Defect Using the Magnetic Sensor Array, PCT/KR2007003801

Lee, J. Y., Hwang, J. S. and Jun, J. W. (2008c) Inspection of Cracks on the Express Train Wheel Using a High Speed Scan Type Magnetic Camera, *Transactions of the KSME Conf*., pp. 31-36

Lee, J. Y., Kim, J. W., Jun, J. W. and Hwang, J. S. (2008d) A Study of the Cylindrical Type Magnetic Camera, *Proceedings of Fall conference of the Korea Society for Nondestructive Testing*, pp. 247-252

Lee, J. Y., Hwang, J. S., Kwon, S. J. and Seo, J. W. (2008e) Inspection of Cracks on the Express Train Wheel Using a High Speed Scan Type Magnetic Camera, *Transactions of the KSME A*, pp. 943-950

Lee, J. Y., Jun, J. W., Hwang, J. S. and Lee, S. H. (2007) Development of Numerical Analysis Software for the NDE by Using Dipole Model, Key *Engineering Materials*, 353-358, pp. 2383-2386

Lee, J. Y., Hwang, J. S., Lee, K. C. and Choi, S. H. (2006a) A Study of Leakage Magnetic Flux Detector Using Hall Sensors Array, *Key Engineering Materials*, 306-308, pp. 235-240

Lee, J. Y., Hwang, J. S., Choi, S. H. and Lim, J. K. (2006b) Detection Probability Improvement for Nondestructive Evaluation Using a Magnetic Camera, *Key Engineering Materials*, 306-308, pp. 241-246

Lee, J. Y., Hwang, J. S. and Choi, S. H. (2006c) The QNDE Using Image Processing of the Magnetic Camera, International *Journal of Modern Physics B*, Vol. 20, Nos. 25-27, pp. 4625-4630

Lee, J. Y., Hwang J. S. and Song, H. R. (2006d) A Study of the Exclusive Embedded A/D Converter Using the Microprocessor and the Noise Decrease for the Magnetic Camera, *Journal of the Korean Society for Nondestructive Testing*, Vol. 26, No. 2, pp. 99-107

Lee, J. Y., Seo, D. W. and Shoji, T. (2004a) Numerical Consideration of Magnetic Camera for Quantitative Nondestructive Evaluation, *Key Engineering Materials*, Vol. 270, No. 1, pp. 630-635

Lee, J. Y., Seo, D. W. and Shoji, T. (2004b) Theoretical Consideration of Nondestructive Testing by Use of Vertical Magnetization and Magneto-Optical Sensor, *KSME International*, Vol. 18, No. 4, pp. 640-648

Lee, J. Y. et al. (2004c) Magnetic Flux Density Apparatus for, e.g., Detecting an Internal Crack of a Metal or a Shape of the Metal, US 6,683,452 B2

Lee, J. Y. et al. (2003) A Display Apparatus of Magnetic Flux Dendity Using 2D Array Magnetic Sensor and 3D Magnetic Fluid, Korea, 10-0376892-0000

Lee, J. Y. and Jun, J. W. (2008a) NDT of Non-Metallic Material Using Penetration of Magnetic Fluid, *Proceedings of Fall conference of the Korean Society for Nondestructive Testing*, pp. 198-202

Lee, J. Y. and Jun, J. W. (2008b) NDT of the Crack on the Austenite Stainless Steel Using the Improved Sheet Type Induced Current and the Linearly Integrated Hall Sensor Array, *Abstracts of 13th ENDE*, p. 48

Lee, J. Y. and Jun, J. W. (2009) Nondestructive Evaluation of Cracks in a Paramagnetic Specimen with Low Conductivity by Penetration of Magnetic Fluid, *NDT & E International*, Vol. 42, pp. 297-303

Smith, C. H., Schneider, R. W., Dogaru, T. and Smith, S. T. (2003) Eddy-Current Testing with GMR Magnetic Sensor Arrays, *AIP Conf Proc*, Vol. 657, No. 1, pp. 419-426